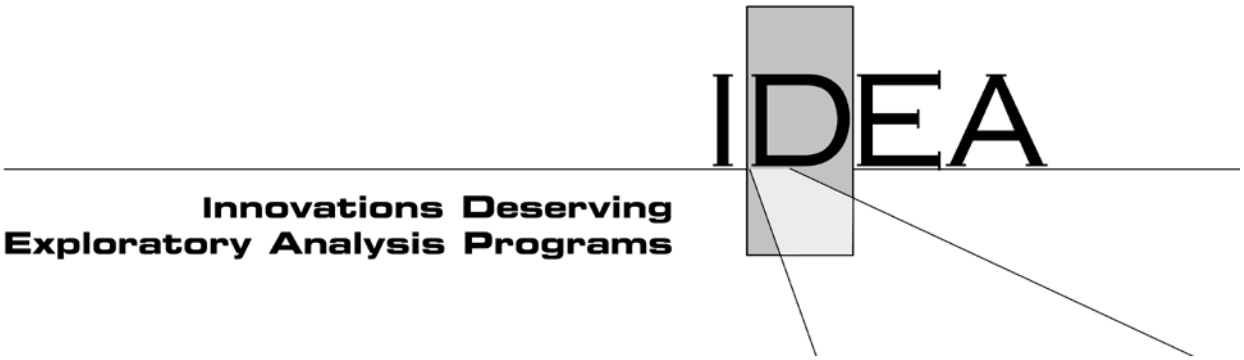

NCHRP IDEA Program

Bio-Inspired "MRI" of Concrete Bridges using Waveform-Based Ultrasonic Tomography

Final Report for
NCHRP IDEA Project 205-A

Prepared by:
Thomas Attard
PowerPolymer, LLC
Didem Ozevin
University of Illinois at Chicago

January 2022

TRB TRANSPORTATION RESEARCH BOARD
The National Academies of
SCIENCES · ENGINEERING · MEDICINE

Innovations Deserving Exploratory Analysis (IDEA) Programs Managed by the Transportation Research Board

This IDEA project was funded by the NCHRP IDEA Program.

The TRB currently manages the following three IDEA programs:

- The NCHRP IDEA Program, which focuses on advances in the design, construction, and maintenance of highway systems, is funded by American Association of State Highway and Transportation Officials (AASHTO) as part of the National Cooperative Highway Research Program (NCHRP).
- The Safety IDEA Program currently focuses on innovative approaches for improving railroad safety or performance. The program is currently funded by the Federal Railroad Administration (FRA). The program was previously jointly funded by the Federal Motor Carrier Safety Administration (FMCSA) and the FRA.
- The Transit IDEA Program, which supports development and testing of innovative concepts and methods for advancing transit practice, is funded by the Federal Transit Administration (FTA) as part of the Transit Cooperative Research Program (TCRP).

Management of the three IDEA programs is coordinated to promote the development and testing of innovative concepts, methods, and technologies.

For information on the IDEA programs, check the IDEA website (www.trb.org/idea). For questions, contact the IDEA programs office by telephone at (202) 334-3310.

IDEA Programs
Transportation Research Board
500 Fifth Street, NW
Washington, DC 20001

Bio-Inspired "MRI" of Concrete Bridges using Waveform-Based Ultrasonic Tomography

IDEA Program Final Report

IDEA Project NCHRP-205-A

Prepared for

IDEA Program
Transportation Research Board
National Academies of Sciences, Engineering, and Medicine

Thomas Attard
PowerPolymer, LLC

Didem Ozevin
University of Illinois at Chicago

January 31, 2022

ACKNOWLEDGEMENTS

This investigation was supported by the National Academics, National Academy of Sciences NCHRP IDEA program under Contract No. NCHRP-205A entitled, “Bio-Inspired "MRI" of Concrete Bridges using Waveform-based Ultrasonic Tomography.” The support from the sponsor is gratefully acknowledged. Any opinions, findings, and conclusions or recommendations expressed in this report are those of the authors and do not necessarily reflect the views of the acknowledged organization. The authors very humbly thank Dr. Inam Jawed, Program Manager of the NCHRP IDEA Program of the Transportation Research Board, for his continued guidance of our research, and for his personal support and friendship over the last four years. We are unboundedly grateful. The authors would also like to thank the Illinois Department of Transportation (DOT) and the Chicago DOT for providing bridge access for this project, and also to the project’s Expert Review Panel – Dr. Tommy Nantung, Dr. Soliman Khudeira, Dr. Liling Cao, Dr. Mohsen Issa, and Richard Gostaustas – for its guidance during quarterly meetings on technology transfer. Finally, the authors thank the exemplary efforts by the graduate research student, Tonghao Zhang, who has remained diligent during the course of this project, displaying unwavering motivation.

TABLE OF CONTENTS

EXECUTIVE SUMMARY

This project developed an innovative measurement and data processing approach of waveform-based ultrasonic tomography to generate tomographic images of sub-surface defects in structural concrete using a single measurement linear wave velocity method and an acoustic nonlinearity coefficient. The evaluation of waveform-based ultrasonic tomography of concrete test specimens led to optimal design parameters of the methodology and appropriate sensor distribution and transmitting signal frequencies. The ultrasonic tomography model was initially developed using numerical data obtained from COMSOL Multiphysics software to simulate concrete damage and to identify an ideal frequency and wave mode to detect subsurface defects. Numerical simulations revealed that inclusions were identified on a tomographic map produced via linear wave velocity using a frequency of 300 kHz and a configuration of 16 arrayed transmitter and receiver sensors. However, linear ultrasonics limits the resolution of the wavelength, especially in heterogeneous materials, leading to the hypothesis that nonlinear ultrasonics and the incorporation of sub-wavelength imaging, or second-order harmonics, will generate tomographic maps (imaging) that reveal improved identification and resolution of subsurface concrete damage. Not only did the study confirm this, but the number of required transmitter and receiver sensors was significantly less using nonlinear versus linear tomography, indicated by the improved resolution of the former in concrete specimens with prescribed inclusions at a depth of 200 mm. Next, linear and nonlinear tomography were compared in a large-scale post-tested concrete-sectioned bridge girder that had been strengthened using a novel hybrid matrix composite (HMC) during hurricane wave-force loading. Nonlinear tomography revealed a significant presence of nonlinearity, indicating deep subsurface damage that conventional linear ultrasonics did not reveal. Lastly, in cooperation with Chicago DOT and Illinois DOT, a field study of a concrete bridge pier for interstate I-55 revealed several pragmatic challenges, including senor coupling and a convoluted cabling architecture, leading to inconsistent measurements. Although nonlinear ultrasonics is fundamentally promising in the detection of deep subsurface concrete damage – indicated by the sudden increase in the measured nonlinearity coefficient through certain cross sections along the height of the pier – additional research is needed to make this approach field-conducive and to allow it to be compared to other NDE methods. In summary, the significant findings of this research are as follows:

(1) Several transmitter-receiver array configurations were identified for concrete to ascertain a viable "resolution-range" to identify inclusion characteristics, e.g., low versus high impedance.
(2) Development of a single-measurement algorithm to obtain linear and nonlinear ultrasonic data.
(3) Acoustic nonlinearity coefficients in ultrasonic tomography to improve defect resolution.

IDEA PRODUCT

The IDEA product is a dual-tomographic software to extract linear and nonlinear ultrasonic images of concrete and to evaluate damage states before and after retrofit using a Hybrid Matrix Composite (HMC) coating. FIGURE 1 shows the measurement components and algorithmic inputs. The measurement components include transmitters and receivers positioned within arrays and a data acquisition system for transmitting and receiving signals. Receivers were tuned to the second harmonic frequency of transmitters for nonlinear ultrasonics. The received signals were decomposed into harmonics using wavelet transform. The fundamental harmonic signal was used to determine a *Time of Flight* (*TOF*) parameter that fed into a linear ultrasonic tomographic analysis. The fundamental and second harmonic amplitudes were used to calculate an acoustic nonlinearity coefficient, which served as the advent of this research for application to concrete as a heterogeneous material, as a second input parameter into the nonlinear ultrasonic tomographic analysis. The dual-tomographic software constructed two images, focusing on different ranges of concrete damage using a single measurement.

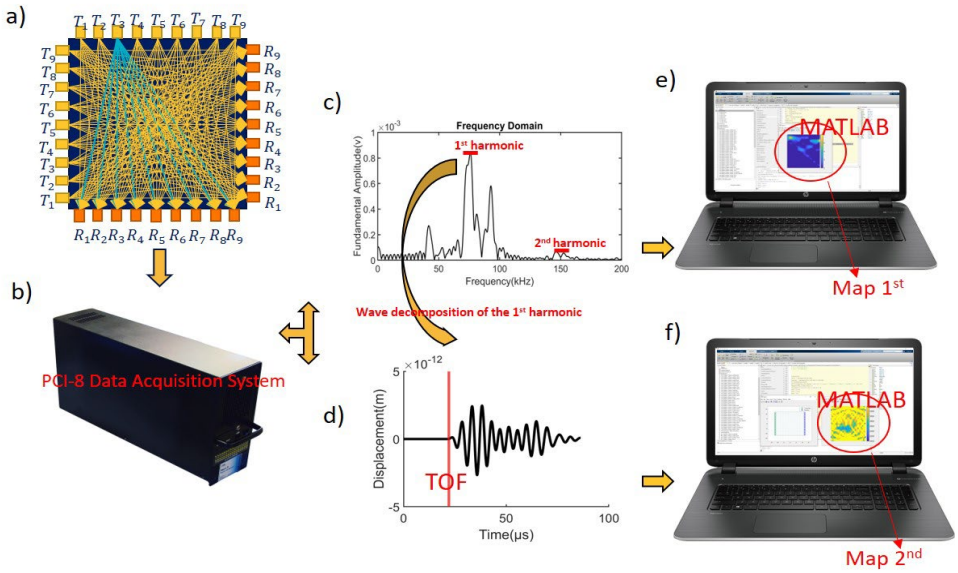

FIGURE 1 Dual Tomography Software: (a) transducer layout for any cross section, T and R represent transmitters and receivers; (b) data acquisition system; (c) frequency spectrum of received signal; (d) time domain signal of the fundamental wave; (e) inputs to acoustic nonlinearity coefficient-based tomography; (f) input to the linear velocity-based tomography.

CONCEPT AND INNOVATION

The innovation of this study is the development of a measurement and data processing approach by using a single measurement to generate tomographic images of subsurface damage in heterogeneous materials

(concrete) using conventional linear wave velocity and an acoustic nonlinearity coefficient. The outcome is improved subsurface damage detection – depth and resolution – in concrete structures.

While a majority of ultrasonic methods in concrete damage analysis is based on local measurement, generation of 3D tomography images can help identify and localize, or discretize, defects, including the type of defect. Various 3D-imaging methods for concrete include coda interferometry using diffusive waves, x-ray computed tomography and microwave imaging. Planes et al. (2013) (1) showed that simple scattering in concrete occurs near a frequency range of 10-100 kHz, whereas multiple scattering was identified near a range of 100-500 kHz; and higher-order scattering was identified at frequencies exceeding 500 kHz, eliciting strong absorption. Zhang et al. (2017) (2) used a diffuse-wave approach to generate 3D imaging of concrete using 16 transmitters and 16 receivers and a frequency range of 80 to 220 kHz. Zielinska and Rucka (2020) (3) developed velocity maps to detect the presence of steel rods and polymer pipe embedded in concrete using 18 transmitters and 18 receivers. However, subsurface resolution of various media, including defects, using linear ultrasonics requires a significant number of transducers, which, furthermore, diminishes at larger measuring depths. Although x-ray computed tomography is a powerful method for assessing concrete damage evolution (4), (5), its field applicability is challenging. Alternatively, microwave imaging requires instrumenting the circumference of concrete with antennas to construct images using a delay-and-sum beamforming approach (6); however, the penetration depth is limited using this method.

Tomography-based methods facilitate mapping internal flaws or material degradation in real-time and *in-situ* without destructive testing. Tomography is achieved by reconstructing the properties of the elastic waves that propagate in a solid medium. Many physical waves may be used for this purpose, for example, visible light, laser, electrical capacitance, resistivity and impedance, X-ray, fluid flow, magnetic induction, and ultrasound (7). However, ultrasonic tomography, more commonly applied to steel, rock and concrete materials, is an attractive alternative in terms of safety, cost-effectiveness, efficiency, and rapid application. However, concrete heterogeneity typically limits the ultrasonic frequency up to 100 kHz when identifying defects (inclusions). To improve resolution, Herman (2009) (8) selected specific properties of ultrasonic waves to reconstruct the tomography image.

The most common linear ultrasonic property that is used to generate subsurface images is the wave velocity. While linear ultrasonics have been successfully used to detect the presence of defects – as opposed to discretizing defects which limits accurate structural prognosed analysis – such as cracking, corrosion, and void in solids, the resolution of these defects is limited by half the wavelength of the excitation frequency. However, nonlinear ultrasonic testing (NLUT) is known to be sensitive to defects because of its use of the sub-wavelength, enabled via higher-order harmonics which was the primary focus of this study for concrete bridges. In NLUT, heterogeneities are mainly measured using three common methods:

acoustoelastic method, nonlinear elastic wave spectroscopy method and higher harmonics method. The higher harmonics method is based on the phenomenon wherein the exciting signal is distorted by the nonlinear (or multi-linear) elastic response of the medium to the incident wave, generating a higher-order, or second, harmonic wave (9). The common nonlinear ultrasonic methods applied to concrete are the second harmonic generation, known as SHG (10) and wave modulation (11). The SHG method is based on the generation of a second harmonic signal in solids upon when the first harmonic wave interacts with heterogeneities. Due to inherent heterogenous characteristic of concrete, typical ultrasonic frequency for the SHG method is 50 kHz (10).

INVESTIGATION

(1) IMAGE RECONSTRUCTION ALGORITHM

Linear Ultrasonics

The tomography of concrete using linear ultrasonics is based on the construction of the wave velocity map. The major measurement variable is *Time of Flight* (*TOF*) between the transmitter and receiver. *TOF* is then converted into wave velocity using the relationship between *TOF* and propagation length.

$$V_{mode} = \frac{L}{TOF_{mode}} \tag{1}$$

In Eqn (1), L is the propagation distance between transmitter and receiver; V_{mode} is the wave velocity of a particular wave mode; and TOF_{mode} is Time of Flight of the wave mode triggered in the structure using an ultrasonic transmitter. Using a constant and known distance between transmitters and receivers, *TOF* may be measured for the linear ray-tracing tomography method. Therefore, an accurate measurement of TOF_{mode} for detecting the same wave mode for different transmitter-receiver distances is critical for developing an accurate tomography map. In general, the most widely used and simplest arrival time pick-up method is threshold-based method. The threshold value is pre-defined, and the first-time signal exceeding the threshold is defined as the *TOF*. The threshold value needs to be set properly to pick up the arrival of the same wave mode. While low computation cost is the advantage of the threshold-based method, it functions less effectively for a signal with low signal to noise ratio and multiple waves. The arrival time pick-up method named outlier-based method was recently developed by the UIC team (12). The outlier is a definition in statistics, which is an observation that lies at an abnormal distance from the other values in a random sample from a population. In this sense, the point off the main signal is considered as the outlier which indicates an abnormal signal. The absolute value of amplitude difference is calculated, and after the entire data set has been obtained, the outlier rule is defined as $\mu \pm 3\sigma$, representing upper and lower limits, where μ is the mean value and σ is the standard deviation. With the outlier-based method, the arrival time

is accurately determined as shown in two examples in FIGURE 2. The image reconstruction algorithm for linear ultrasonics is similar to the computed tomography. A typical tomography inversion model includes two methods: ray-based (3) and waveform-based (13). The ray-based method is typically used for engineering materials due to its advantage of lower computational cost. The outcome of this method is the construction of a velocity distribution map, and the primary experimental input to the algorithm is TOF.

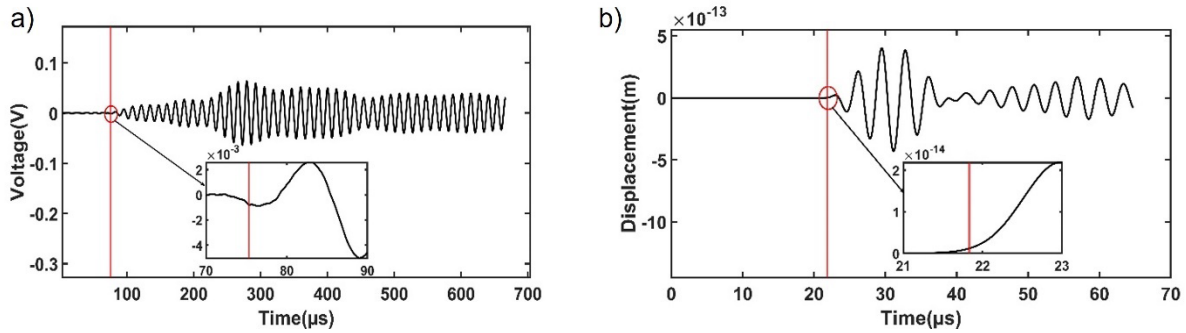

FIGURE 2 The arrival times of two waveforms highlighted with a red line by the outlier-based method: (a) the arrival time of the experimental waveform; and (b) the arrival time of the numerical waveform.

The geometry is discretized in a certain pixel depending on the ray paths. The interpretation of pixel is such that the model is divided into a number of uniform grids, where each grid is considered to be a single pixel, and TOF within each pixel may be calculated as

$$TOF_i = \sum_{i=1}^{n} l_{ij} * S_j \tag{2}$$

where i indicates any ray path; S_j represents the slowness within pixel, j, and is the inverse of velocity, s/m; n is the total number of rays as a function of the transmitters and receivers; and l_{ij} is the length of ray-path i within a single pixel j. The layout of transmitters and receivers is defined by green and blue patterns, respectively. The path of wave propagation passing through each pixel is illustrated in FIGURE 3. The model is built such that the ray path is considered to be a straight path between transmitters and receivers, and the slowness, or velocity, in each pixel remains constant. Multiple wave paths are constructed. A uniform mesh may be created using N lines by N rows. The pixel index is shown in FIGURE 3b. To obtain the information of the entire distribution map, Eqn. 2 may be expanded into matrix form as

$$\begin{Bmatrix} TOF_1 \\ TOF_2 \\ \vdots \\ TOF_n \end{Bmatrix} = \begin{bmatrix} l_{11} & l_{12} & \cdots & l_{1m} \\ l_{21} & l_{22} & & l_{2m} \\ \vdots & & \ddots & \vdots \\ l_{n1} & l_{n2} & \cdots & l_{nm} \end{bmatrix} \begin{Bmatrix} S_1 \\ S_2 \\ \vdots \\ S_m \end{Bmatrix} \tag{3}$$

where m is total number of the pixels, $m = N \times N$ in this mesh; n indicates the total number of wave paths depending on the number of the transmitters and receivers. Iterative methods are commonly used to solve

the linear equation, which has been based on the back-projection updating procedure, algebraic reconstruction technique (ART method) and simultaneous iterative reconstruction techniques (SRIT). In this study, the ART method was used to solve Eqn. 3. The algorithm involved two steps: (1) obtaining the $[L]$ matrix depending on the number and placement of sensors, where the TOF measurement served as input to Eqn. 3; and (2) solving the linear equation using the ART algorithm. The open-source tool (AIR) associated with MATLAB was used, where the output variable S, the slowness, inverse of the velocity, provided a velocity visualization within each pixel. The tomography of the sample was accordingly reconstructed.

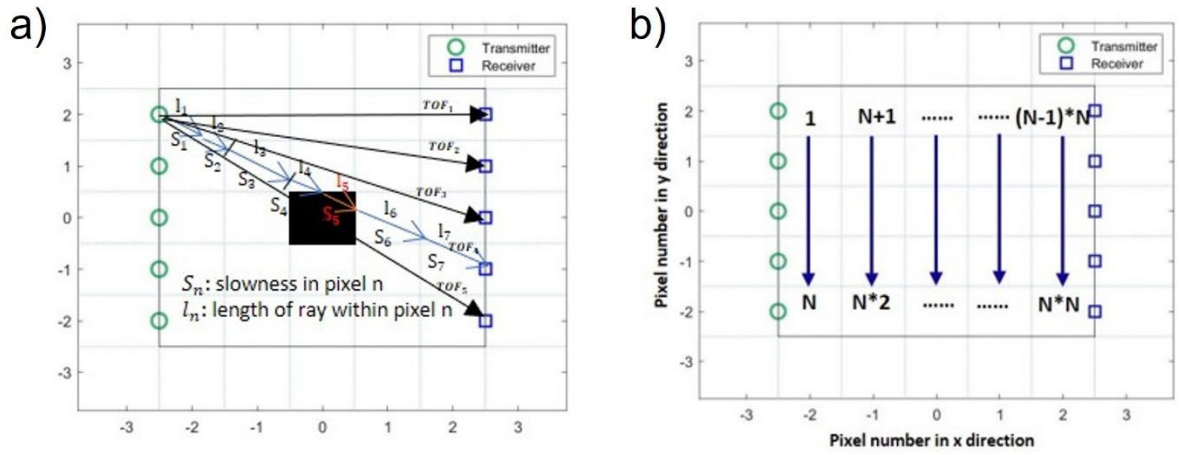

FIGURE 3 (a) Schematic of straight ray path on a two-dimensional geometry; and (b) the regulation of pixel index.

Nonlinear Ultrasonics

The acoustic nonlinearity coefficient is the critical parameter used to describe the ultrasonic nonlinear phenomenon. The second and the third order acoustic nonlinear coefficients are commonly applied to defect heterogeneities in solids (14). The second order nonlinearity coefficient, β_{theory}, is proportional to the ratio of the second harmonic amplitude and the square of first harmonic amplitude, defined as

$$\beta_{theory} = \frac{8A_2}{{A_1}^2 xk^2} \tag{4}$$

where A_1 and A_2 are the first and second harmonic amplitudes; x is the wave propagation distance; and k indicates the wave number of the first harmonic wave. Acoustic nonlinearity coefficient β_{theory} is proportional to the voltage amplitudes ${A_2}^v/(A_1^v)^2$ when distance and wave number are constant. The experimental nonlinearity coefficient is calculated as

$$\beta = \frac{{A_2}^v}{(A_1^v)^2 xk^2} \tag{5}$$

Following the method developed by Mostavi et al. (2017) (15), the first and second harmonic waveforms are decomposed as shown in FIGURE 4.

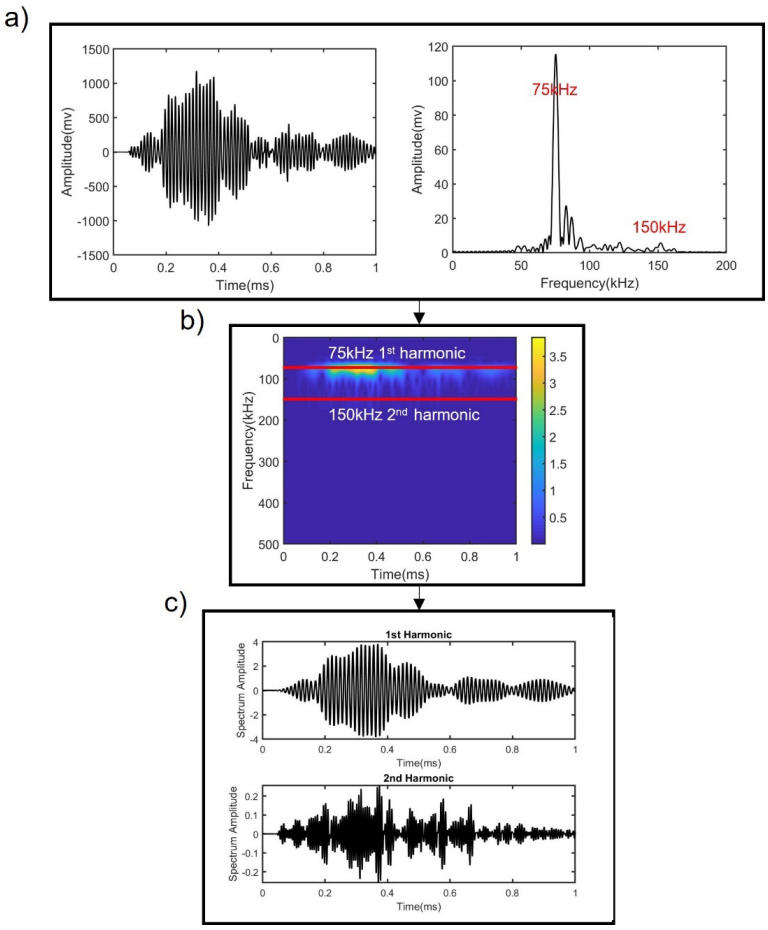

FIGURE 4 The schematic to obtain the acoustic nonlinearity coefficient, (a) the received signal in time domain and its frequency spectrum, (b) spectrogram indicating 1st harmonic and 2nd harmonic frequencies, and (c) time domain signals of 1st harmonic and 2nd harmonic frequencies extracted from spectrogram.

FIGURE 4a shows the received time domain signal and its frequency spectrum. The first harmonic frequency at 75 kHz and second harmonic frequency at 150 kHz are highlighted on the spectrogram shown in FIGURE 4b. The time domain signal of each harmonic was extracted from the spectrogram and plotted in FIGURE 4c. The amplitudes of the first and second harmonic signals served as inputs to the calculation of the acoustic nonlinearity coefficient as shown in Eqn. 5.

For the nonlinear tomography image, the variable used to reconstruct tomography images was changed from a velocity-based parameter to a nonlinearity parameter. FIGURE 5 illustrates that multiple wave paths pass through a single pixel, where each path is associated with a β value. Within one pixel, instead of using the wave velocity as in linear ultrasonics, a weighted acoustic nonlinearity coefficient value C was defined

and measured as the summation of the product of each ray length in a single pixel and β (value) that is associated to each ray and used to evaluate the nonlinearity distribution map.

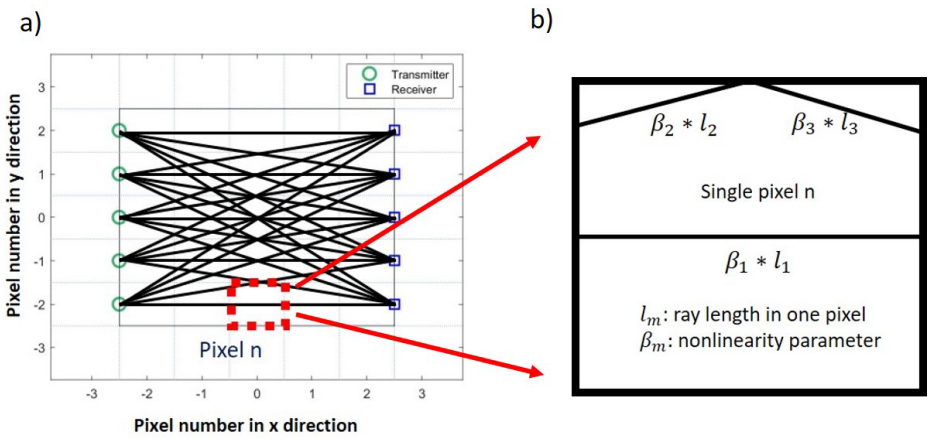

FIGURE 5 Schematic of acoustic nonlinearity parameter in each pixel, (a) ultrasonic paths and (b) acoustic nonlinearity coefficients within one pixel.

The value of C may be calculated as

$$C_j = \sum_{j=1}^{m} l_{ji} \times \beta_i = \sum_{j=1}^{m} l_{ji} \times \frac{8A_2^{vi}}{(A_1^{vi})^2 l_i k_i^2} \tag{6}$$

where i and j indicate the total number of paths and pixels, respectively; m is the total number of pixels; A_1^i and A_2^i are the first and second harmonic amplitudes for each ray path i; k_i is the wave number of first harmonic wave in ray path i, which is calculated as

$$k_i = \frac{2\pi}{\lambda_i} \tag{7}$$

where λ_i is the wavelength of the first harmonic wave in path i. It can be obtained by

$$\lambda_i = \frac{V_{pi}}{f} \tag{8}$$

where V_{pi} is the phase velocity of the first harmonic wave in path i; f is the frequency in the first harmonic. The first harmonic wave velocity in each path can be calculated using the parameter TOF which is extracted in the linear ultrasonic tomography as

$$V_{pi} = \frac{l_i}{TOF_i} \tag{9}$$

where l_i is the length in ray i and TOF_i is measured using the outlier method as illustrated in FIGURE 2. Similar to the linear tomography method, Eqn. 6 may be expressed in matrix form as

$$\begin{Bmatrix} C_1 \\ C_2 \\ \vdots \\ C_m \end{Bmatrix} = \begin{bmatrix} I_{11} & I_{12} & \cdots & I_{1m} \\ I_{21} & I_{22} & & I_{2m} \\ \vdots & & \ddots & \vdots \\ I_{n1} & I_{n2} & \cdots & I_{nm} \end{bmatrix}^T \begin{Bmatrix} \beta_1 \\ \beta_2 \\ \vdots \\ \beta_n \end{Bmatrix} \tag{10}$$

Consequently, the nonlinear tomography image is created based on the C-vector.The nonlinear tomography parameter was obtained using the same sensor array as the linear tomography parameter in order to generate two images simultaneously. The schematic of the dual measurement approach is illustrated in FIGURE 6.

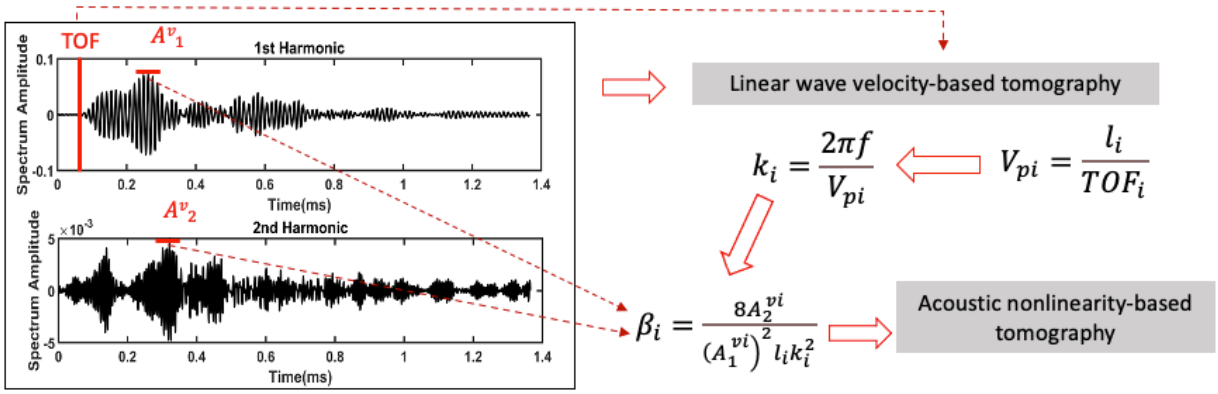

FIGURE 6 The schematic for calculating inputs for linear wave velocity-based and acoustic nonlinearity-based tomography images.

After the time history signal has been decomposed into harmonics using wavelet transform, the arrival time of the first harmonic signal is determined using the outlier-based method, where TOF is the input in Eqn. 5. The wave number k may be obtained using the wave velocity which utilized the TOF in the first harmonic wave, see Eqn. 9. The amplitudes of the first and the second harmonic frequencies and k are used to calculate the acoustic nonlinearity coefficient as the β inputs to Eqn. 10. With this hybrid approach, two tomographic images of linear wave velocity-based and acoustic nonlinearity-based may be generated for a single measurement.

(2) NUMERICAL RESULTS

Numerical models using COMSOL Multiphysics software were designed to evaluate the tomography algorithm and to understand the resolution of linear ultrasonic tomography. To reduce the computational time, a 2D plane strain model was selected, representing the cross-section of the cuboid concrete geometry. The excitation signal was a five-cycle sine wave function with a Hanning window. Two frequencies (100 kHz and 300 kHz) were tested to understand the frequency-dependent resolution. The concrete geometry was a square shape with the length of 75 mm, and modeled with varying size and inclusion forms, see FIGURE 7. The length of the inclusion was increased from 15 mm to 25 mm. The parameter TOF was

influenced by two factors: the distance between the transmitter and receiver, and the presence of inclusions in the ray path. The transducers were modelled as points and displayed evenly along the side of model. Finite element analysis was made using a free triangular mesh with a mesh size of 0.965 mm. The mesh size was selected as one-twelfth of a wavelength. The material properties are summarized in TABLE 1.

TABLE 1 Material Properties used in Numerical Simulations

Properties	Base material	Inclusion (EPS foam)	Inclusion (rebar)
Density (kg/m^3)	2300	34	7,850
Young's Modulus (Pa)	25 x 10^9	3.7 x 10^7	200 x 10^9
Pressure Wave Velocity (m/s)	3,400	2,300	5,000
Acoustic Impedance Ratio to Concrete	1	0.01	5

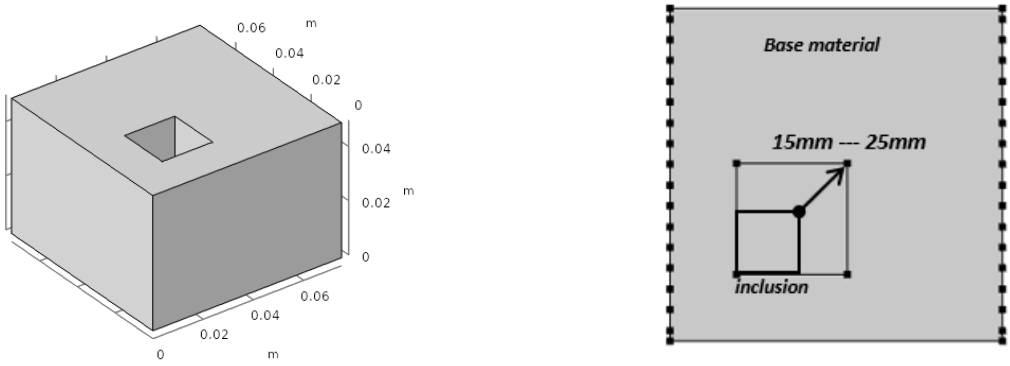

(a) (b)

FIGURE 7 The geometry of the model (a) the profile of cuboid sample; and (b) 2D cross section profile.

To evaluate the optimum resolution of detected inclusions, which depends on the pixel resolution, three models with different transducers were built. The number of pixels in one direction was selected as the same value as the number of transducers because the number of pixels was highly dependent on the selected transducer layout. For example, an 8×8 pixels image was created when eight transducers were attached along one direction. An image post-processing approach through interpolating the points between each pixel was implemented. The cubic interpolation of values at neighboring points in each respective dimension was applied to eliminate the distinct boundary between neighbor pixels. The approach was applied to the image constructed using an excitation frequency of 300 kHz and a 16x16 transducer array. FIGURE 8 shows that the image enhancement improves inclusions visualization.

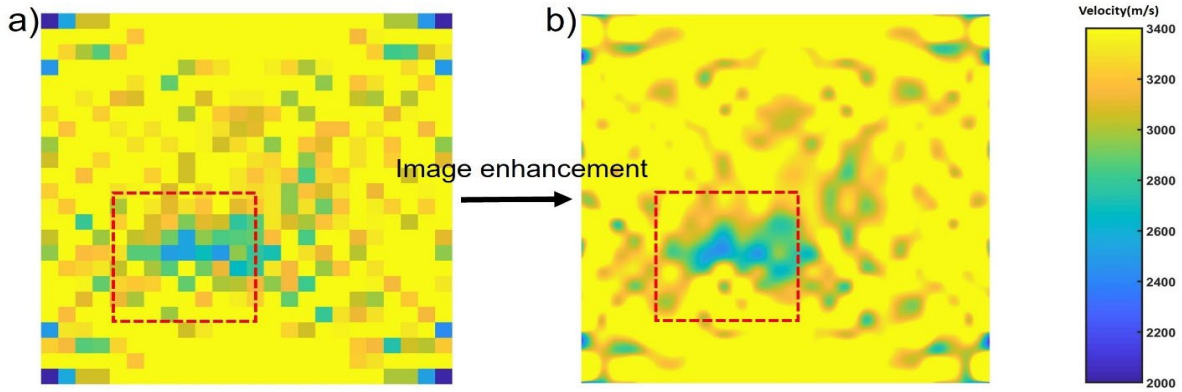

FIGURE 8 An example of linear wave velocity-based tomography of concrete with foam inclusion highlighted with red dashed line: (a) original image; and (b) enhanced image.

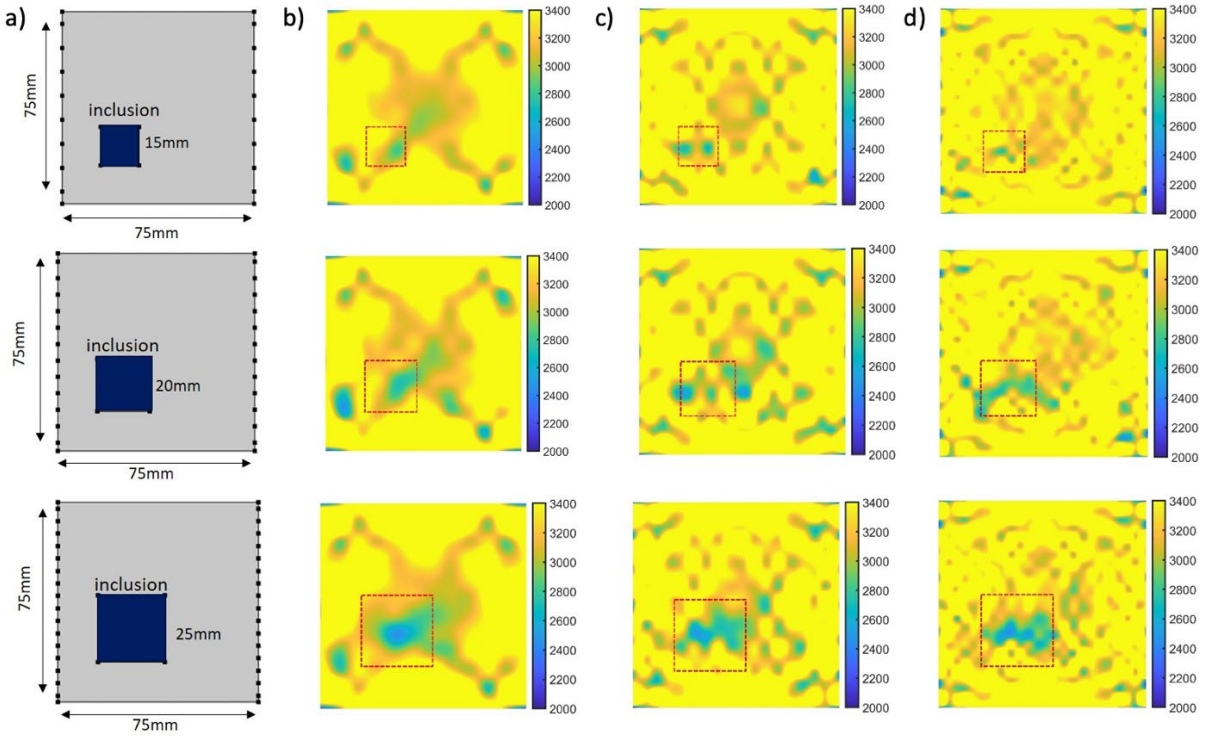

FIGURE 9 The simulation results of the 300 kHz excitation frequency: (a) the dimensions of inclusions; (b) the tomography image of 8x8 transducer array; (c) 12x12 transducer array; and (d) 16x16 transducer array.

It is important to note that this method does not affect the resolution and accuracy of the tomography algorithm. The tomography results of the transducer layouts for 8x8, 12x12 and 16x16 are shown in FIGURE 9(b), (c) and (d), respectively. The dark blue square highlights the presence and location of an inclusion. Inclusion sizes 20 mm and 25 mm were clearly detected for both 12x12 transducer and 16x16 transducer array configurations. However, a comparison of the resolutions of defects in a sample with a 15 mm inclusion netted a fuzzy image. The wavelength of 300 kHz frequency in concrete is approximately 15

mm, and therefore, detectability using a frequency of 300 kHz is approximately one-half, or 7.5 mm. Consequently, a higher transmitter frequency is needed to more clearly detect inclusion sizes of 15 mm, where concrete heterogeneity limits the frequency to prevent scattering and absorption. A larger number of transducers can enhance the resolution and image quality.

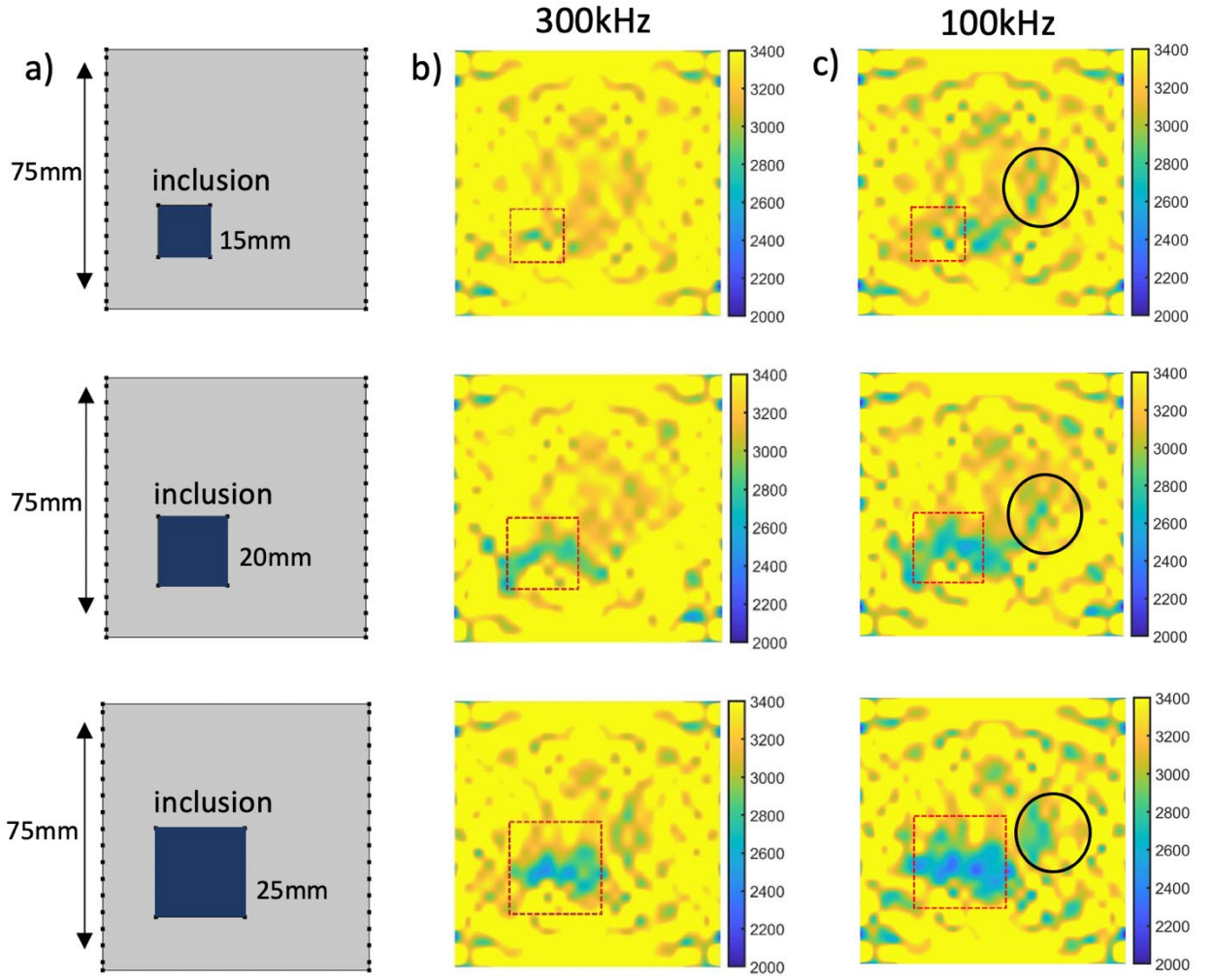

FIGURE 10 The influence of excitation signal to the tomography result using 16x16 transducer array and three inclusion sizes: (a) the profiles of models; (b) the tomography images using 300 kHz excitation signal; and (c) the tomography images using 100 kHz excitation and black circles indicate the artificial heterogeneities due to the algorithm.

In summary, the performance of linear wave velocity-based tomography significantly depends on the transducer layout, excitation frequency and acoustic impedance of the detected inclusion with respect to the base material. The number of sensors affects the resolution and the quality of images although it may be limited by the physically available space to fit the sensors along concrete edges as well as by the depth of the defect, like in many commercially available NDE methods. While higher excitation frequency improves the resolution, the heterogeneous characteristic of concrete may cause scattering and absorption

of ultrasonic waves and produce inaccurate image reconstructions. The detectability of inclusions increases when the ratio of acoustic impedance of base material to the inclusion is further away from unity, and, obviously, when the size of the inclusion with respect to base material increases.

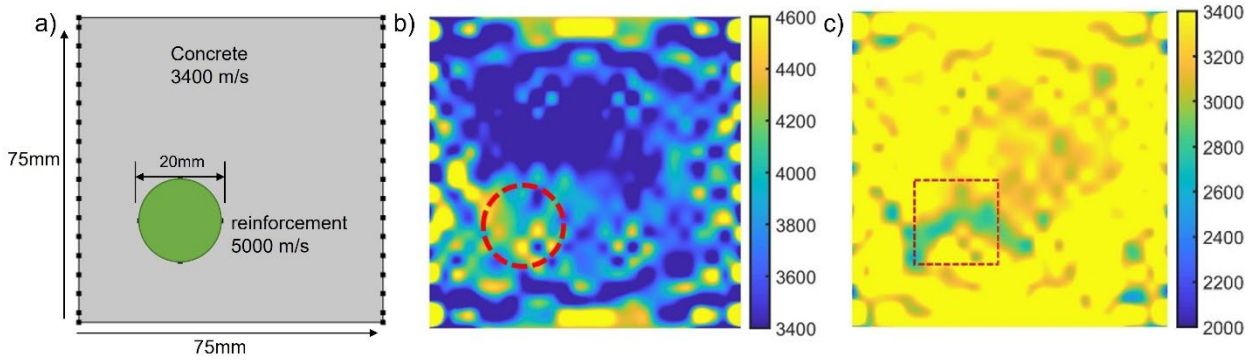

FIGURE 11 Linear wave velocity-based tomography for different inclusion impedances: (a) numerical model; (b) constructed image of model with reinforcement; and (c) constructed image of model with foam inclusion.

(3) LABORATORY MEASUREMENTS – SAMPLES WITH INCLUSIONS

Three concrete samples were constructed at the UIC laboratory. The samples included pure concrete, concrete with rebar (for studying corrosion) and concrete with EPS inserts as shown in FIGURE 12.

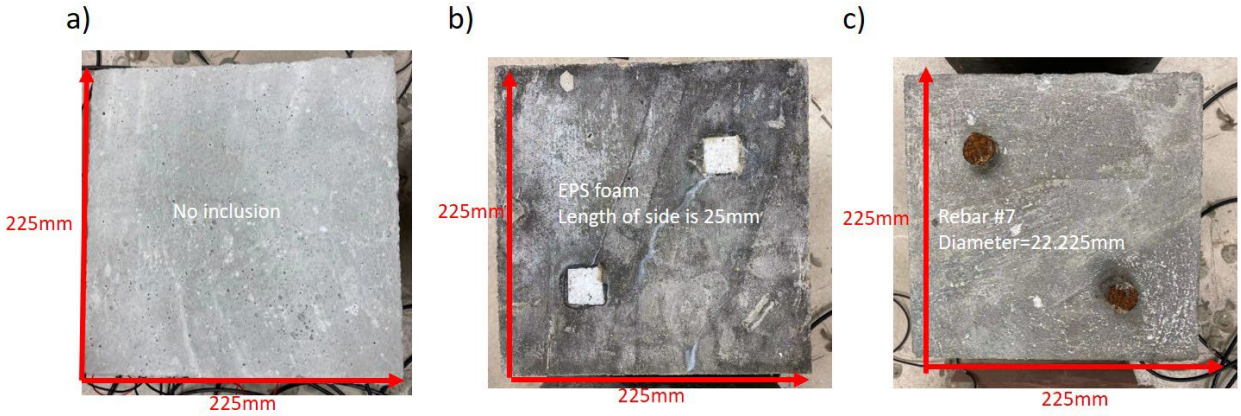

FIGURE 12 Plane views of three samples: (a) pure concrete sample without inclusions; (b) concrete with #7 reinforcements; and (c) EPS foamed concrete sample.

The ultrasonic measurements were performed using three concrete samples with the dimensions as 225 mm×225 mm×200 mm. The first sample was a pure concrete without any inclusion and used as a benchmark sample. EPS (expanded polystyrene insulation) foam with 25 mm side length was inserted through the concrete sample in the second sample. The third concrete sample contained two #7 reinforcements (diameter as 22.2 mm). The mixture proportions are given in TABLE 2.

TABLE 2 Concrete Mixture Proportions

Material	Coarse Aggregate	Natural Sand	Holcim Cement	GBBF Slag	Water
1.5 cubic ft concrete mix, lbs.	107.00	68.28	22.50	7.50	12.50

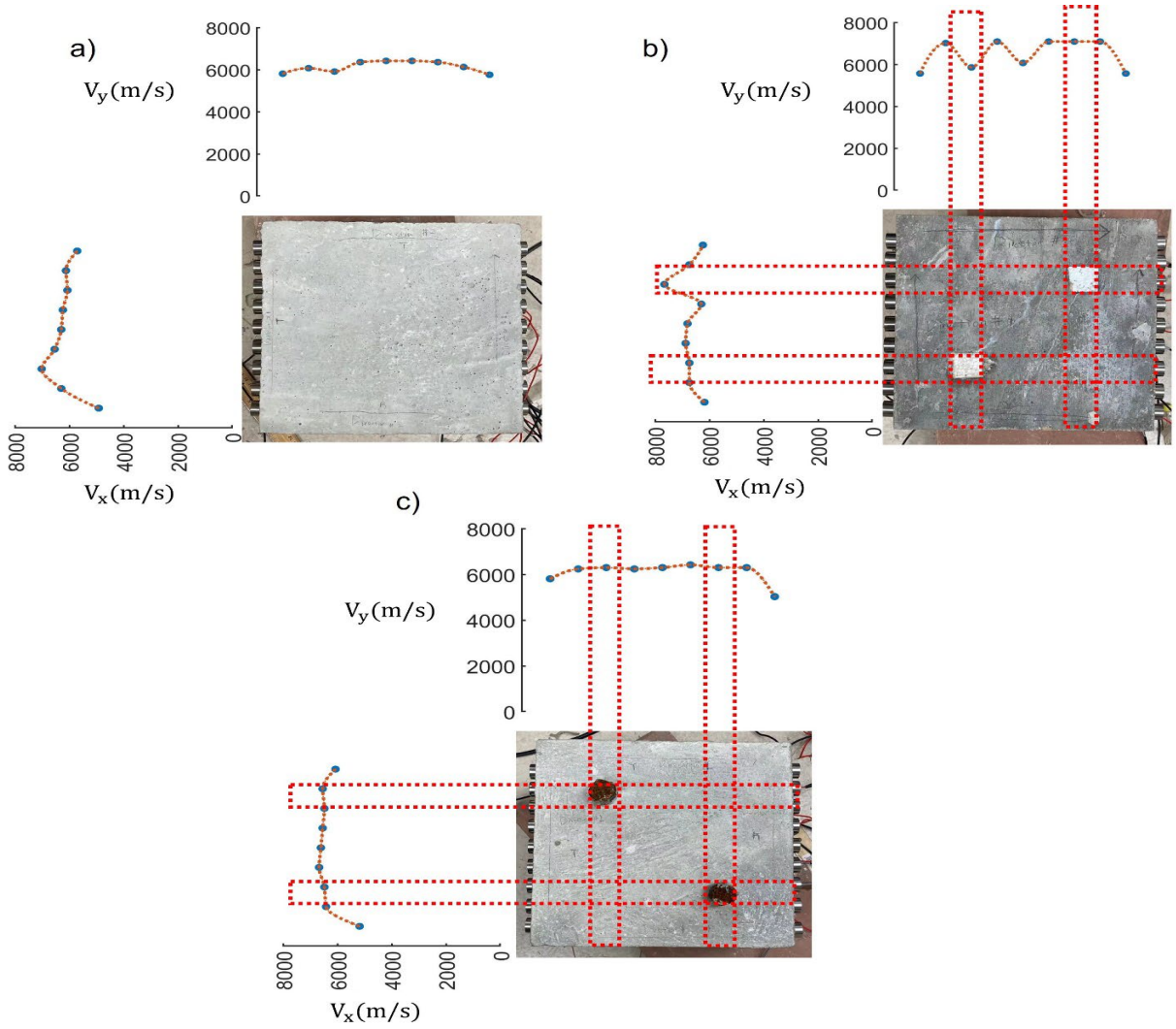

FIGURE 13 The wave velocities obtained from the direct path of transmitter-receiver pairs: (a) pure concrete; (b) concrete with two EPS foams; and (c) concrete with two reinforcements.

The measurements were taken after the specimens were cured in a moisture room for 28 days. To understand the sensitivity of wave velocity to inclusions, the direct-path measurements were evaluated. The direction between the transmitter to the receiver at the proper opposite surface were defined as the direct path. The results of the wave velocity of each testing point are shown in FIGURE 13. The wave velocity remains almost constant for all the points in pure concrete except at the third testing point in the x direction as shown in FIGURE 13a. As depicted in FIGURE 13b and c, a drop occurred at the third testing points in the y

direction of concrete with foam. However, most paths passing through inclusions have no significant change in the wave velocity. Ultrasonic tomography images were generated as shown in FIGURE 14 for linear wave velocity-based tomography. The first column shows the concrete samples.

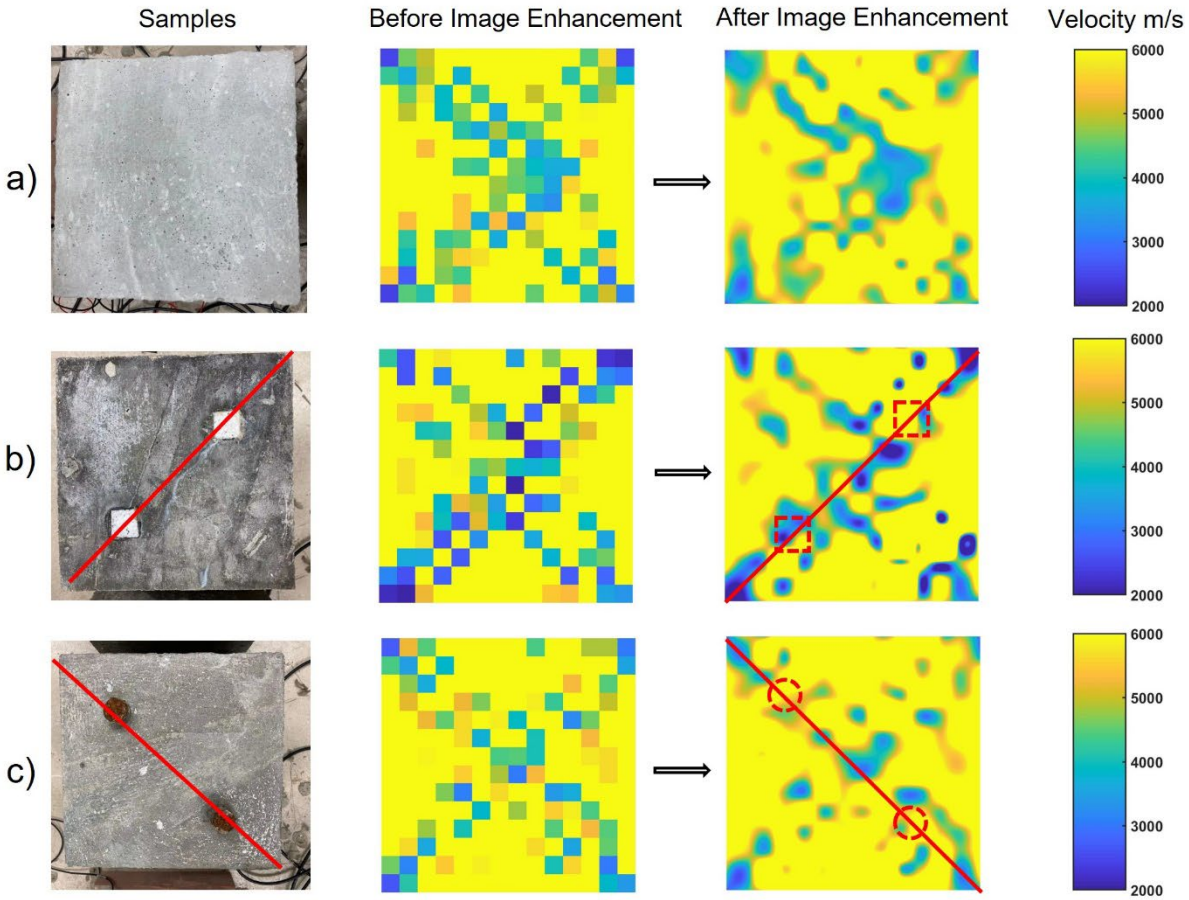

FIGURE 14 The experimental linear wave velocity-based tomography images of three concrete samples: a) pure concrete; (b) concrete with two EPS foams; and (c) concrete with two reinforcements.

The second column and third column indicate the results before and after image enhancement. The fourth column shows the scale. The images were constructed using the 162 wave paths. Due to the limited number of sensors and the low excitation frequency, linear wave velocity-based tomography could not detect the positions of EPS foams and reinforcements. However, the pure concrete has no dark blue region whereas concrete with EPS foams reveals several dark blue pixels along the diagonal line, indicating the decrease in wave velocity. The percentage of heterogeneity in the image increases with the presence of EPS foam. Similar to numerical models, the percentage of light blue region drops, and some light blue pixels eliminate as compared with tomography of pure concrete because the velocity of ultrasonic in reinforcement is faster than in concrete. As compared to the linear ultrasonic results, the direct path results of the nonlinearity

parameter elicit distinct changes at the coordinates of the inclusions. As shown in FIGURE 15a, the nonlinearity parameter appears with a minor variance in the pure concrete.

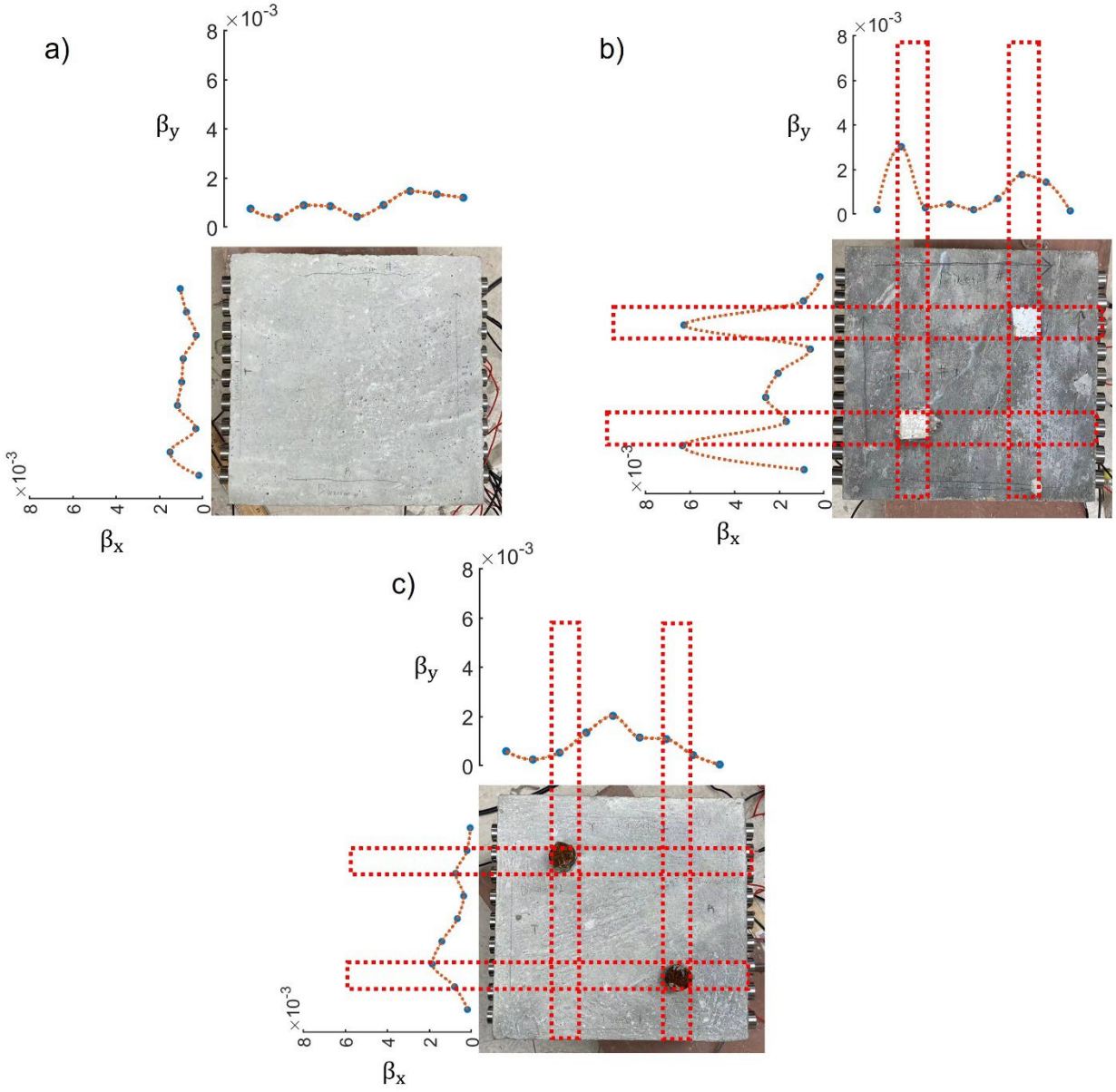

FIGURE 15 The acoustic nonlinearity parameters obtained from the direct path of transmitter-receiver pairs on concrete specimens: (a) pure concrete; (b) concrete with two EPS foam sections; and (c) concrete with two rebars (reinforcement).

The value of the nonlinearity parameter rises when wave propagates through foam in both orientations and through reinforcement in the x-direction as observed in FIGURE 15b and c, indicating that the nonlinearity parameter β increases by due to the presence of inclusions. The nonlinear ultrasonics could not pinpoint the vertical positions of rebars especially at the top-left corner. This could be due to the coupling between rebar and concrete during construction leading to a scatterer source to prevent the detection of higher

harmonics; however, this also indicates a limitation as such coupling issues may occur in practice. FIGURE 16 shows the tomography images reconstructed by the weighted acoustic nonlinearity coefficient C. The range of the weighted acoustic nonlinearity coefficient is defined as 4×10^{-4} to 12×10^{-4} for the pure concrete and the concrete with two EPS foams and as 6×10^{-4} to 12×10^{-4} for the concrete with reinforcements.

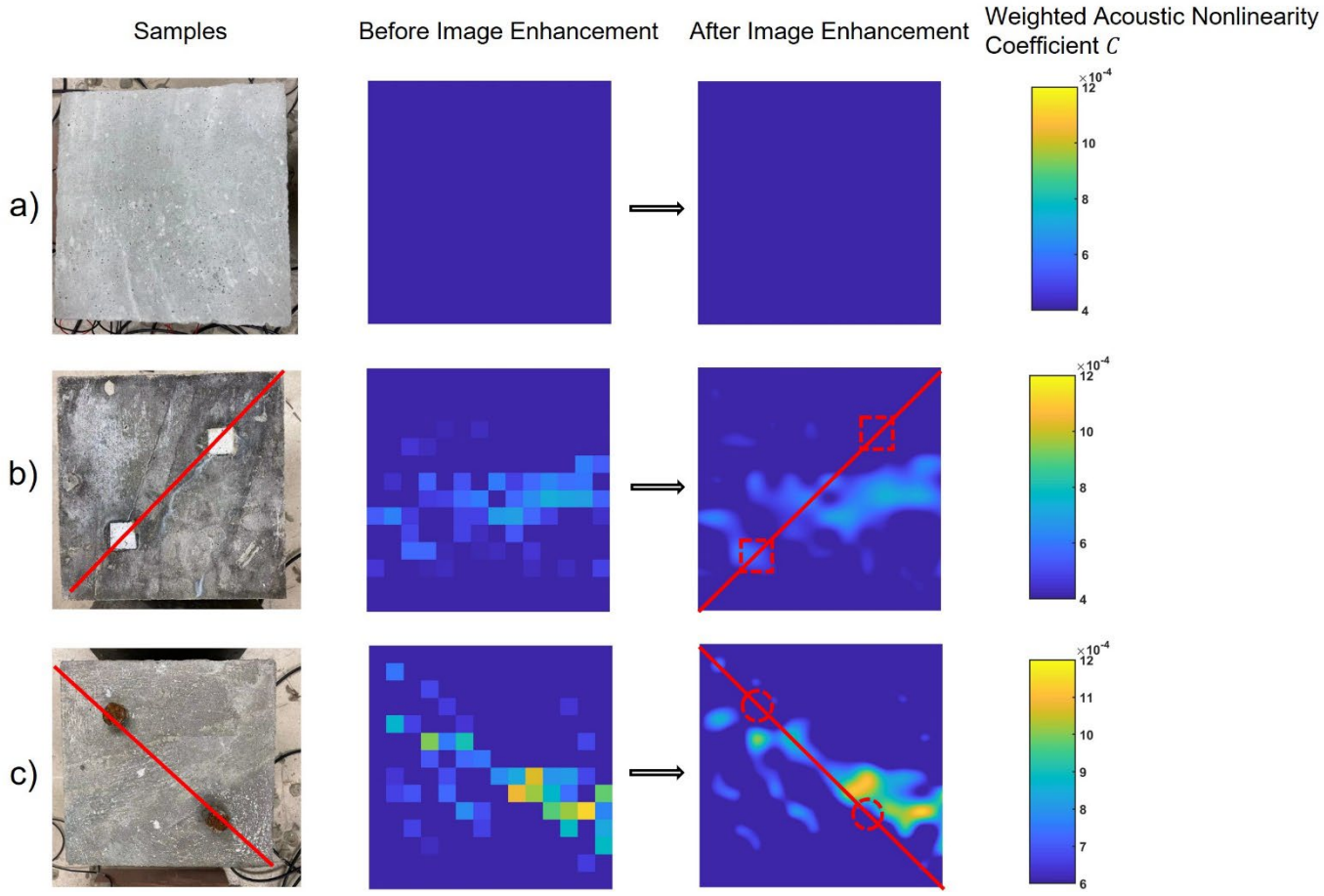

FIGURE 16 The experimental weighted acoustic nonlinearity coefficient-based tomography images of three concrete samples: a) pure concrete; (b) concrete with two EPS foams; and (c) concrete with two reinforcements.

The lower bound of the scale is set as 4×10^{-4} to create a clearer image to differentiate the concrete and heterogeneities as the majority of weighted acoustic nonlinearity coefficient for concrete ranges from 0 to 4×10^{-4}. The mean values and standard deviations of weighted acoustic nonlinearity coefficient C are listed in TABLE 3. The lowest mean value and standard deviation are obtained for the pure concrete, whereas the concrete with reinforcements reaches the highest values. The tomography of pure concrete has a uniform acoustic nonlinearity coefficient close to the lowest scale number as shown in FIGURE 16a. For the case of the concrete with EPS foams, clearer image to differentiate the regions of heterogeneities is obtained as compared to linear ultrasonic tomography. The blue region represents the homogenous concrete

whereas the light blue region indicates heterogeneities. The position of the foam at the left corner was accurately detected using nonlinear ultrasonic tomography. However, a shift in the location of the foam to the right corner was observed which may be due to the interference of the two foams' proximity. As depicted in FIGURE 16c, the detection of reinforcements was successful compared to the use of linear ultrasonics. The region with brighter color indicated higher nonlinearity, which coincided with the location of the various rebars. The results indicated that nonlinear ultrasonic tomography can detect high-density inclusions and also accurately localize them as compared to linear ultrasonic tomography.

TABLE 3 Weighted Acoustic Nonlinearity Coefficients of Concrete Samples

Weighted Acoustic nonlinearity coefficient C	Pure concrete	Concrete with foam inclusions	Concrete with reinforcements
Mean Value	1.67×10^{-4}	2.95×10^{-4}	3.81×10^{-4}
Standard Deviation	9.07×10^{-5}	1.77×10^{-4}	2.72×10^{-4}

(4) LABORATORY MEASUREMENTS – GIRDER WITH DAMAGE

Two-dimensional tomography imaging was taken from the concrete girders strengthened with the HMC polymeric coating and loaded for twelve cycles; the girder was forcibly failed ("lifted") after testing in order to detach its connection-details from the cap beam, as shown in FIGURE 17 (red section near the support).

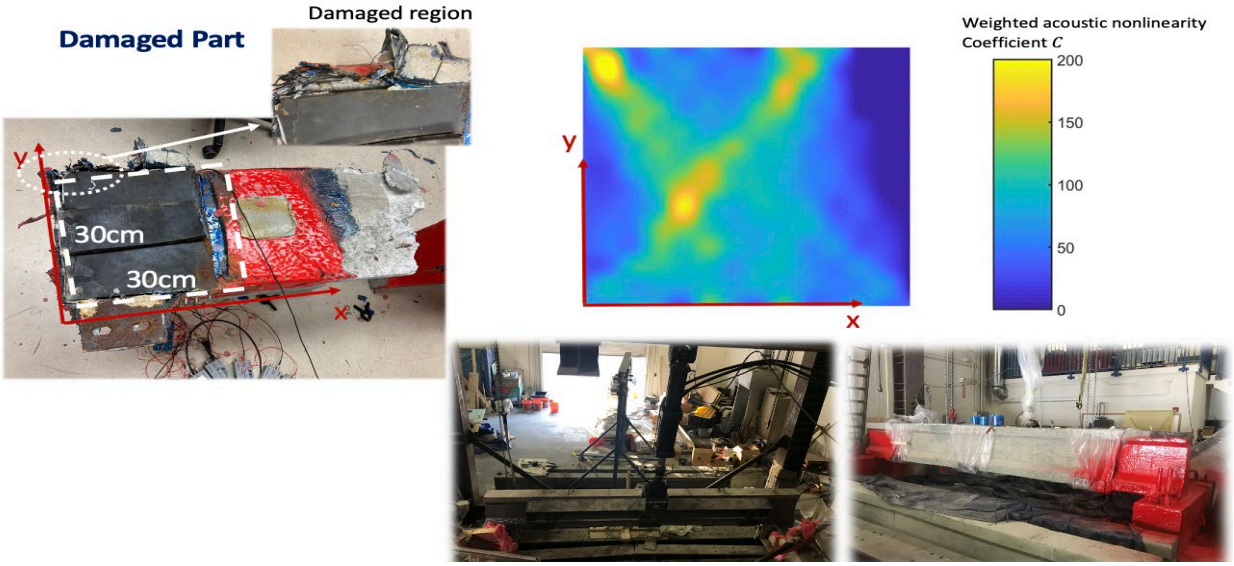

FIGURE 17 Nonlinear ultrasonic tomography measured from the damaged section of concrete girder. The support section was strengthened using the HMC polymer coating prior to loading.

The nonlinear ultrasonic tomography was obtained similar to three calibration samples presented for the concrete samples. Nine R6 sensors (transmitters) were attached using hot glue and used to generate an excitation signal of 75 kHz; and nine R15 sensors (receivers) were attached to the opposite surface using

hot glue, detecting an ultrasonic wave of 150 kHz. FIGURE 17 shows images of the damaged section where the ultrasonic array was attached along x-direction, and the ultrasonic wave propagated along the y-direction. The image used the weighted acoustic nonlinearity coefficient as the variable indicated that damage had initiated from corners propagating in the diagonal direction to indicate large shear stress during the post-test detachment stage. The measurement was repeated at the undamaged section of concrete girder as shown in FIGURE 18**.** A low acoustic nonlinearity coefficient value was calculated, indicating no damage at the undamaged section. To further validate the nonlinear ultrasonic tomography, the concrete girder was numerically modeled and the experimental loading scheme was applied to determine the maximum stress direction as an indication of damage orientation.

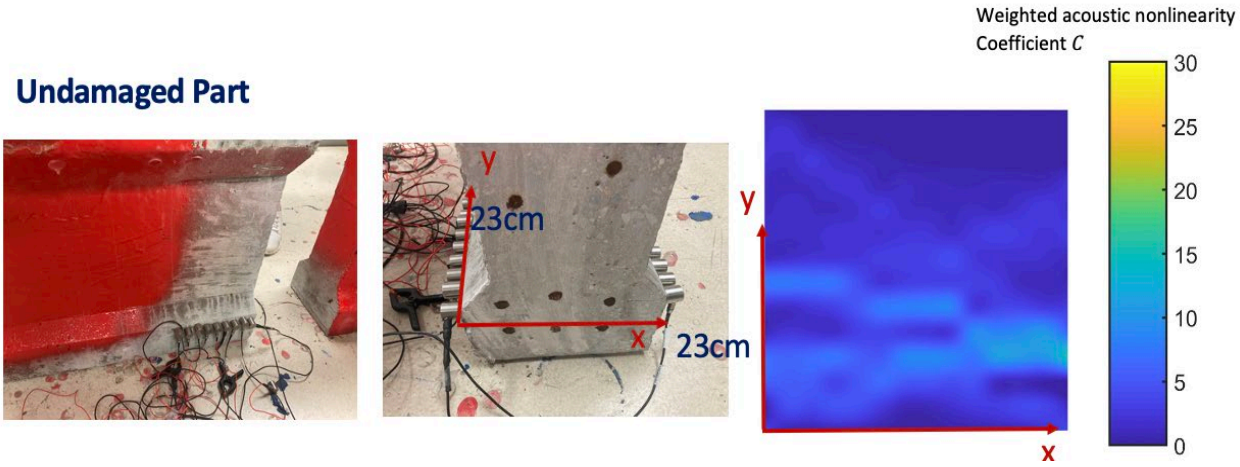

FIGURE 18 Nonlinear ultrasonic tomography measured from the undamaged section of concrete girder.

Structural dynamic response of the tested girder was studied numerically to validate the experimental results. A numerical model was developed using COMSOL Multiphysics to predict the structural behavior of the concrete girder under dynamic loading. The concrete girder was modeled as a rigid connection to the cap beam; the details are shown in FIGURE 19. The girder length was 4.57 m. A cyclic wave-load load function (hurricane loading) similar to the experiment was defined. The loading time-history is depicted in FIGURE 19(c). The peak force was calculated as 160.1 kN. The force-controlled load function was composed of a 5-second load cycle, where the force increased from 0 to 2.5-seconds, where it remained for 1 second before decreasing to zero within 1.5-seconds. Five-point loading (3 force points and 2 reaction points) were simulated and located along the span, where one loading point was located at center-span, and each of two other load points was located 1.5m to n either side. FIGURE 19(b) shows the profile view of loading angle at 76 degrees with respect to the horizontal plane in order to simulate Hurricane Katrina slamming wave and rising surge forces. Damping of the HMC coating was considered at the ends of girder as 20% based on previous Dynamic Mechanical Analysis while the remaining part of girder was assigned a conventional 5% structural damping of concrete (16), (17).

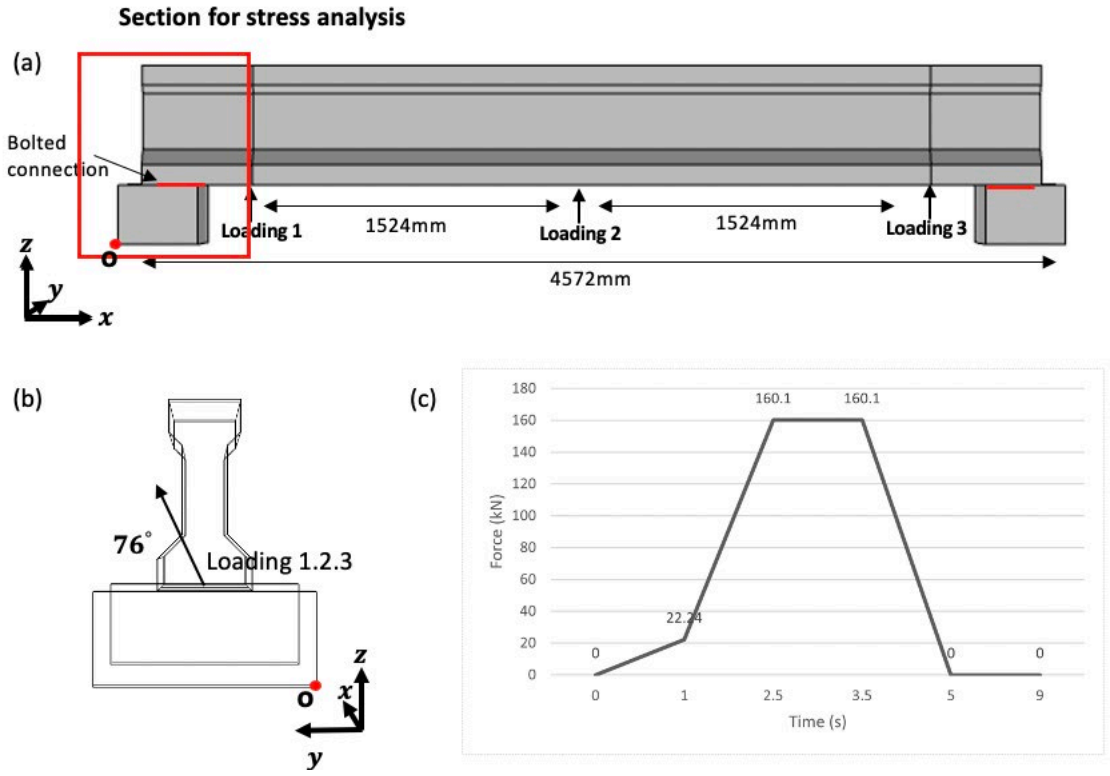

FIGURE 19 Numerical model of the damaged girder: (a) girder span and loading points; (b) side view of the loading angle; and (c) the loading function.

FIGURE 20 depicts a von Mises stress distribution at the girder-end after 3.5 s of loading. Large von Mises stresses were observed along the diagonal plane highlighted in in FIGURE 20. It is near the edge of the cap beam and girder. von mises stresses range from 0 up to $8e7\ N/m^2$. The highest stress is close the top edge of the bottom surface, gradually reducing to approximately $3e7\ N/m^2$ along the plane. The potential failure plane agrees with the tomography results depicted in FIGURE 17.

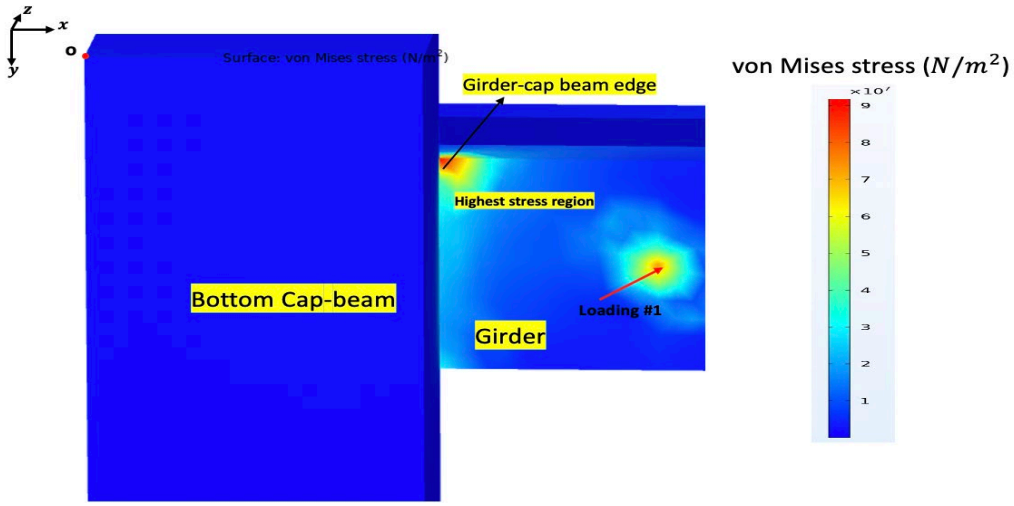

FIGURE 20 von Mises stress distribution at the left end of girder at 3.5 seconds.

FIELD DEMONSTRATION

The field measurement was taken from a concrete pier of multi girder steel bridge that supported the I-55 highway at the intersection of Ashland Avenue and 31st Street as shown in FIGURE 21. This bridge was selected in collaboration with Chicago DOT and Illinois DOT due to its easy access points in addition to the fact that a visual inspection of surface cracking was observed that intimated potential subsurface damage / cracking (and potential rebar corrosion). Similar to the laboratory test set-up, R6 and R15 sensors were used as transmitters and receivers, respectively. The cross section of the concrete pier was 70 cm x 70 cm. In order to cover entire section, 9 x 9 sensor array was positioned at two lines across the section. A total of 256 ray paths were collected from each cross section. The measurements were taken at three different locations along the height of the pier. The sensors were coupled to the concrete surface using vacuum grease.

FIGURE 21 The location of bridge pier under I-55 (left), a photo of bridge piers (middle) and a photo of the bridge pier measurements taken (right).

FIGURE 22 shows the position of the level 1 sensors, which is away from the intimated corrosion indicators. This first assessment was made using a direct way path between transmitter (left side of section) and receiver (right side of section). The relationship evinces an acoustic nonlinearity coefficient at each path. In general, the acoustic nonlinearity coefficient is below 0.02, which is lower than the damaged post-tested concrete girder. High nonlinearity was measured at three paths as indicated by the red circles. However, the signal to noise ratio was very low at these paths, resulting in substantial divergence. As an example, the waveform that was recorded along path 13 is shown in the figure. No ultrasonic wave propagated along this path. A potential explanation for this was the inconsistent sensor coupling due to the field conditions, the condition of the concrete surfaces, and the reinforcement. These are plausible explanations for the wave scattering that was observed.

FIGURE 23 shows the position of level 3, which is close to the concrete section where concrete had previously spalled (visually) and there was apparent rebar corrosion. A comparison to section 1 reveals a

larger nonlinearity coefficient below 0.2 near paths 1 through 10, which is ten times larger than the nonlinearity observed at level 1. A significant increase in the nonlinearity coefficient is observed at path 7 while the signal-to-noise ratio is acceptable.

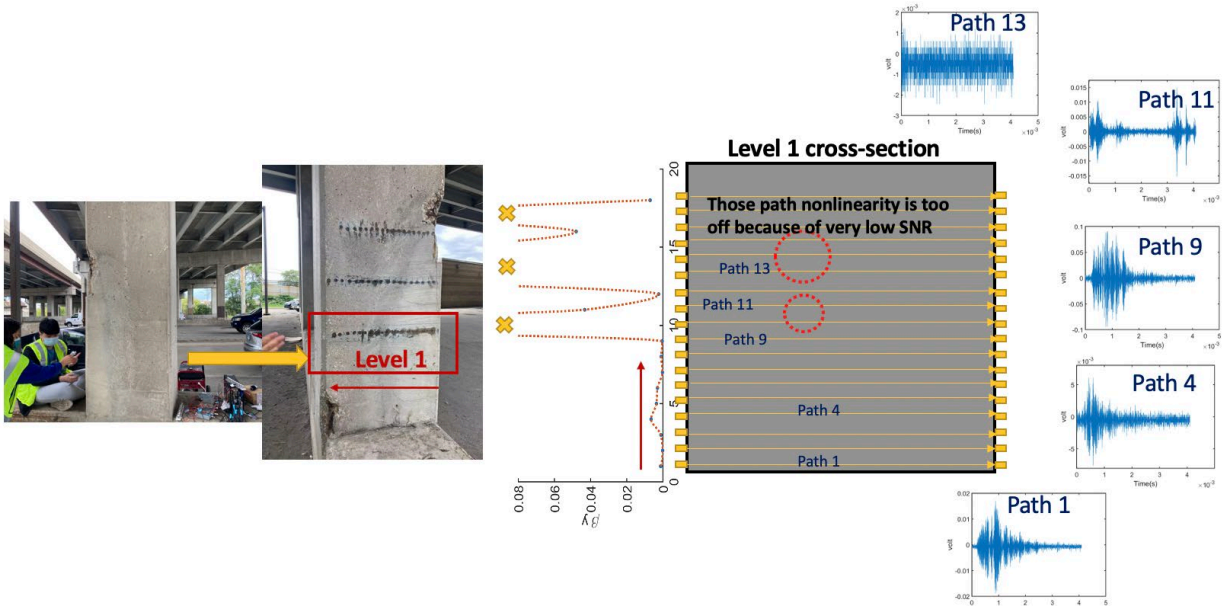

FIGURE 22 The position of level 1 (left) and the direct path result (right).

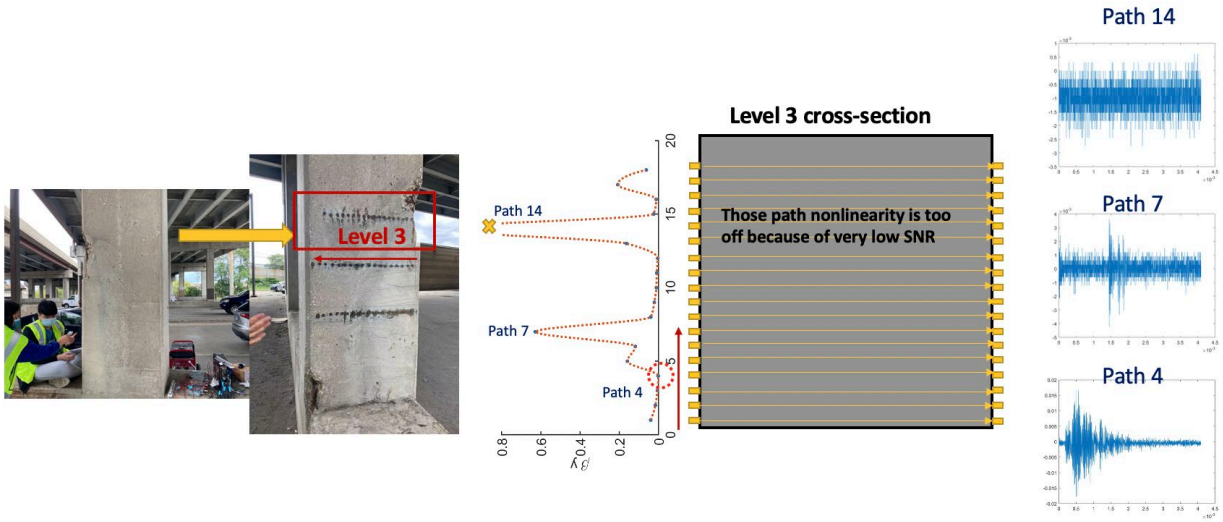

FIGURE 23 The position of level 3 (left) and the direct path result (right).

Path 14 has another artificial increase in the nonlinearity coefficient due to low signal to noise ratio as observed from the waveform. The relative comparison of levels 1 and 3 indicates that higher nonlinearity is detected at level 3, which agrees with the visual observation of corrosion at this level. Sudden increases of the nonlinearity coefficients were measured at certain positions, which should be validated using other

NDE methods, specifically at near-surface depths in order to be confident in the baseline predictions of the other NDE methods.

Three main challenges were faced in this field-measurement phase of the research as shown in FIGURE 24. First, ultrasonic tomography requires an array of transmitters and receivers. Resolution of defects is proportional to the number of sensors employed. In this study, a 9 x 9 sensor array was attached to the sensor carrier. The receivers were re connected to external pre-amplifiers, which were connected to data acquisition system using several individual cables. Cabling was not only excessively time-consuming, but it also proved to be overly convoluted for field application due to the many overlapping cables. In fact, a single error made in the array configuration may result in incorrect measurements. The second challenge was the coupling. vacuum grease was used to couple the sensors; the removal of hot glue from the concrete surfaces was excessively difficult and time-consuming. additionally, the set time of hot glue was longer than the vacuum grease-based attachment. conversely, trying to ensure consistently good coupling from the array of receivers was difficult using the vacuum grease due to the self-weight of the long array of sensors, resulting in some sensors disconnecting from the surface. a mechanism to ensure a constant pressure on the array is needed. the third challenge was trying to ensure a consistent direct path between the transmitters and receivers, positioned at two opposing concrete faces. to circumvent this, a tape measure was used along the two sides of the pier to ensure parallel paths. however, this approach would be challenging at taller heights along the pier.

(a) (b) (c)

FIGURE 24 The challenges faced at the field measurement: (a) cabling; (b) coupling; and (c) ensuring direct path between transmitters and receivers.

PLANS FOR IMPLEMENTATION

The plans for implementation first require addressing the three main challenges during field testing. The following suggestions are provided:

- Multiplexer Design: To reduce the convoluted cabling, a sensor array may be connected to a multiplexer such that only one cable will be connected to the data acquisition system. This approach would also reduce the cost of instrumentation because only one receiving channel would be sufficient. In this case, the signal of each ray may be separated using a time-delay approach.
- Sensor Array on a Flexible Cable: By using a greater number of sensors, the defect resolution improves. A sensor array attached on a flexible printed circuit board (PCB), as shown in FIGURE 25, may be manufactured to serve as an alternative to placing sensors directly on the concrete surface. Plus, a single PCB would reduce the number of cables to one that will be connected to the data acquisition system.

- Software Development: A software with Graphical User Interface may be designed to reduce the computational time of the tomography.

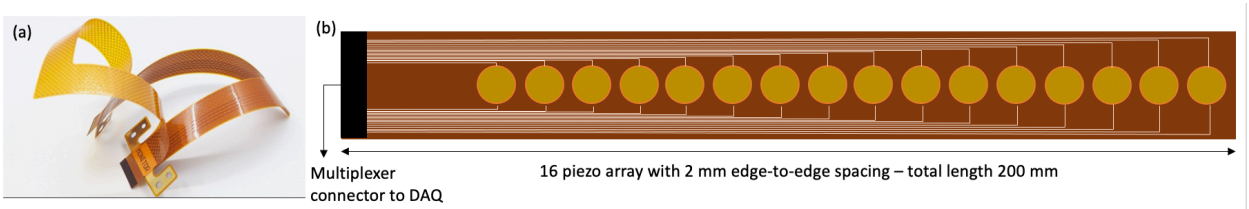

FIGURE 25 Flexible printed circuit board (PCB): (a) single-cable design ready for convenient plug-in to a multiplexer (https://www.pcbgogo.com/knowledge-center/Flexible_PCBs.html); and (b) PCB with 16 piezoelectric wafers.

CONCLUSIONS

An integrated (combined) measurement approach of linear and nonlinear ultrasonic tomography was developed to localize subsurface defects in (heterogeneous) concrete test samples, a large-scale concrete post-tested sectioned girder that had been previously strengthened using a Hybrid Matrix Composite (HMC) polymeric coating, and a field application on a concrete pier. The same sensor array was used for the two former tests and measurements, where the received signals were decomposed into their respective harmonics in order to generate inputs for linear wave velocity-based tomography and acoustic nonlinearity coefficient-based tomography. The tomography models were developed under an assumption that the ray path was straight between transmitters and receivers. The linear wave velocity image was developed such that total slowness in each path was calculated as the summation of the slowness within each pixel region that the path previously passed. It was numerically shown that the image resolution of linear wave velocity-based tomography was limited by the number of transmitters and receivers, which was limited by the physical available space around each concrete specimen and the size of the sensors, which ultimately limited the resolution and depth of subsurface defect that could be discretely identified. To circumvent this

imitation, an acoustic nonlinearity coefficient image was also reconstructed using a variable defined as the weighted acoustic nonlinearity coefficient, which was calculated by the multiplication of each ray length within each pixel and its associated β value along the respective ray. The two tomographic methods were shown to be sensitive to the impedance ratio of the base material to the identified inclusion. The combination of linear and nonlinear ultrasonic images, where the former finds and the latter refines the images, appears promising for the identification of subsurface defects at larger depths.

INVESTIGATOR PROFILES

Dr. Thomas Attard, President and CEO of PowerPolymer, LLC, received his Ph.D. in 2003 from Arizona State University. He is a former Associate Professor from the University of Alabama at Birmingham. Dr. Attard's expertise includes multi-hazards resilience and smart city sustainability using unique co-cure polymer composites with interfacial chemical bonds whose properties scale to bulk properties, including energy transferability. Dr. Attard's research has been supported by Dept. of Energy, Dept. of Homeland Security, National Academy of Sciences (NCHRP IDEA 205-A), Federal Highway Admin, and Dept of Transportation. He holds two patents on a unique isophorone diisocyanate amine surface modification (IEPM). His company is starting a new project in Atlanta through JC&J Developments to spray IEPM (HMC) coatings on fifty new multi-million-dollar homes, followed by two projects: Multi-hazards protection of multi-family dwellings and Hurricane protection of single-family homes in FL and SC.

Dr. Didem Ozevin, Professor at University of Illinois at Chicago, received her Ph.D. in 2005 from Lehigh University. Her expertise includes structural inspection, periodic structural design, acoustic emission, nonlinear ultrasonics, novel sensors for damage detection. She developed and taught a new course in Fall 2020 on Structural Inspection using UAVs. She received the NCHRP IDEA award in 2012 to measure the cumulative stress in plate-like structures using nonlinear ultrasonics. Several journal and conference proceedings were published, and the project led to additional funding from NSF. While the method was tested at two bridges in VA and IL, the resolution required to detect stress limited successful implementation in bridges. She is a recipient of ASNT Faculty Award in 2014 and NSF CAREER Award in 2016.

REFERENCES

(1) T. Planès and E. Larose. Cement and Concrete Research A review of ultrasonic Coda Wave Interferometry in concrete, Cement and Concrete Research, Vol 53, 2013, pp. 248–255.

(2) Y. Zhang, E. Larose, L. Moreau, and G. d'Ozouville. Three-dimensional in-situ imaging of cracks in concrete using diffuse ultrasound, Structural Health Monitoring, Vol. 17, No. 2, 2017, pp. 279-284.

(3) M. Zielinska and M. Rucka. Detection of debonding in reinforced concrete beams using ultrasonic transmission tomography and hybrid ray tracing technique, Vol. 262, 2020, pp. 120104.

(4) W. Tian and N. Han. Evaluation of Meso-damage Processes in Concrete by X-Ray CT Scanning Techniques Under Real-Time Uniaxial Compression Testing, Journal of Nondestructive Evaluation, Vol. 38, No. 2, 2019, pp. 1–12.

(5) X. Liu, D. Sun, D. Liu, K. Meng, C. Ni, Z. Shao, and L. Sun. Simulation of ultrasonic propagation in porous cellular concrete materials, Construction and Building Materials., Vol. 285, 2021, pp. 122852.

(6) E.A. Jiya, N.S.N. Anwar, and M.Z. Abdullah. Detection of Cracks in Concrete Structure Using Microwave Imaging Technique, International Journal of Microwave Science and Technology. Vol. 2016.

(7) P. Grangeat, *Tomography*. John Wiley & Sons, Inc., New York, 2013.

(8) G. T. Herman, *Fundamentals of Computerized Tomography: Image Reconstruction from Projections*. Springer Science & Business Media (Springer Publishing Company), New York, 2009.

(9) K.Y. Jhang, C.J. Lissenden, I. Solodov, Y. Ohara, and V. Gusev. *Measurement of Nonlinear Ultrasonic Characteristics*. Springer Publishing, New York, 2020.

(10) C. Yang and J. Chen. Cement and Concrete Research Fully noncontact nonlinear ultrasonic characterization of thermal damage in concrete and correlation with microscopic evidence of material cracking, Cement and Concrete Research, Vol. 123, July 2019, pp. 105797.

(11) Y. Xu, Q. Wang, X. Jiang, H. Zu, W. Wang, and R. Feng. Nondestructive assessment of microcracks detection in cementitious materials based on nonlinear ultrasonic modulation technique, Construction and Building Materials, Vol. 267, 2021, pp. 121653.

(12) L. Zhang, J. Dong, V. Godinez-Azcuaga, O. Ley, E. Lowendar, H. Saboonchi, and D. Ozevin. The identification of accurate and computationally efficient arrival time pick-up method for acoustic tomography, Proceedings SPIE 10971, Nondestructive Characterization and Monitoring of Advanced Materials, Aerospace, Civil Infrastructure, and Transportation XIII, April 1, 2019, pp. 39.

(13) P.C. Hansen and J.S. Jørgensen. AIR Tools II: algebraic iterative reconstruction methods, improved implementation, Numerical Algorithms, Vol. 79, No. 1, pp. 107–137, 2018.

(14) M. Zhao, Z. Nie, K. Wang, P. Liu, and X. Zhang. Nonlinear ultrasonic test of concrete cubes with induced crack, Ultrasonics, Vol. 97, 2019, pp. 1–10.

(15) A. Mostavi, N. Kamali, N. Tehrani, S. Chi, D. Ozevin, and J. E. Indacochea. Wavelet based harmonics decomposition of ultrasonic signal in assessment of plastic strain in aluminum, Measurement, Vol. 106, 207, pp. 66–78.

(16) T.L. Attard and L. He. Linking Nanoscale Chemical Changes to Bulk Material Properties in Polymer Composites subject to Impact Dynamics, ACS Applied Materials & Interfaces, Vol. 11, No. 22, 2019, pp. 20404 – 20416.

(17) L. He, T.L. Attard, H. Zhou, and A. Brooks. Integrating Energy Transferability into the Connection-Detail of Coastal Bridges using Reinforced Interfacial Epoxy-Polyurea Reaction Matrix Composite, Composite Structures, Vol. 216, 2019, pp. 89-10.

APPENDIX

RESEARCH RESULTS

Project Title: Bio-Inspired "MRI" of Concrete Bridges using Waveform-based Ultrasonic Tomography
Project Number: NCHRP-205-A
Project Start Date: October 1, 2020
Project Completion Date: March 31, 2022
Product Category: Bridge Preservation

Principal Investigator: Thomas Attard, Ph.D.
Title: President and CEO, PowerPolymer, LLC
E-Mail: thomas.attard@powerpolymer.net
Phone Number: 480 - 878 - 0002

TITLE: Mapping subsurface damage in concrete bridges

SUBHEAD: Subsurface concrete damage was mapped using novel nonlinear acoustics on an ultrasonic tomography platform to design spray-on retrofit coatings

WHAT WAS THE NEED? This research was developed to enhance post-construction maintenance of concrete bridges using accurate subsurface defect identification. The method, a bio-inspired ultrasonics methodology applied to heterogeneous materials, developed an integrated linear-nonlinear tomography technology to reduce cost and time expended to perform Bridge Ratings in aging concrete bridges. The research addressed high-priority agency, industry and contractor needs, helping decision-makers to accurately assess the health of the 9.1% of bridges that are structurally deficient or to re-assess potentially misevaluated bridges to either leave them alone, retire them, or to develop a preservation solution.

Ostensibly, the linear and nonlinear integrated-measurement ultrasonic tomography represents significant improvement to alternative, yet conventional, non-destructive evaluation (NDE) techniques due to large penetration depth and high resolution of defects. The tool aids end-users by accurately diagnosing component damage and prognosing short- and long- term health in the advent of a preservation program, including a hybrid matrix-composite (HMC) a spray-on coating.

WHAT WAS OUR GOAL? The research goal was to accurately identify and map deep subsurface damage in concrete bridge girders at high resolution using, initially, coupon-scale concrete samples, secondly, large-scale post-tested bridge girder, and thirdly an actual Chicago-city bridge. The third test brought to light a need to make the MRI technology field-conducive.

WHAT DID WE DO? The primary research objective is an integrated linear-nonlinear ultrasonic tomography methodology to map subsurface defects using the same sensor array for linear and nonlinear measurements, where received signals were decomposed into harmonics to generate subsequent inputs for linear-wave velocity-based tomography and acoustic nonlinearity coefficient-based tomography. Two sub-objectives were consequently directed: (1) Develop numerical models of the linear and nonlinear integrated-measurement ultrasonic tomography, including design of optimal waveform-based ultrasonic technology, at large penetration depths that conventional NDE methods cannot capably identify; and (2) Test the optimal linear-nonlinear tomography technology by mapping subsurface damage in a large-scale post-tested HMC-retrofitted concrete bridge girder. The task of bringing the technology to practical light was supported by Chicago DOT and Illinois DOT via use of an I-55 concrete bridge pier.

WHAT WAS THE OUTCOME? The linear-nonlinear tomography model assumed a straight ray path between transmitters and receivers but which also required an excessive number of transmitters and receivers to compute acoustic nonlinearity coefficients in order to feed them into the multiple linear analyses. The limited amount of physical space around a given concrete component made this a practical infeasibility, confirmed by the field study. In addition to necessitating large-sized sensors that revealed surface coupling challenges – mainly on account of their weight – the linear-nonlinear tomography method is not practical in its current logistical form. Notwithstanding, its laboratory-scale accuracy, in terms of ascertaining deep subsurface damage in coupon-scale and large-scale concrete specimens in real-time confirmed its strong potential as a viable NDE tool for end-users, including state agencies performing bridge inspections. To address the tool's practical limitations, additional research is needed. One idea that will be proposed involves devising a sensor array printed on a flexible printed circuit board to house a large number of sensors. In this light, a single multiplexer design could eradicate the convoluted-cable architecture dilemma by using a single cable connected to a data acquisition system. This would not only reduce the cost of this already inexpensive NDE technology, but it would convert the linear-nonlinear tomography technology into a practical option. To test this hypothesis, a research plan that proposes the use of a single-cable sensor-array architecture for field-feasibility is suggested.

WHAT IS THE BENEFIT? The immediate benefit to the public is the cost savings for state agencies who procure this emerging linear-nonlinear tomography as an NDE technology. Long-term cost-savings include longer life-cycles for aging bridges via accurate damage detection and custom retrofit solutions. Although the HMC coating is a rapid-retrofit technology that limits traffic and lane closures and alleviates safety risk to construction personnel, the linear-nonlinear tomography has logistical feasibility challenges that need to be addressed before moving forward with public implementation.

LEARN MORE

More details are provided in the final report posted on the NCHRP IDEA website. The Final Report is also available via the **link** to PowerPolymer Solutions' website: https://www.powerpolymer.net/recent-research-equipment-procurement using the password **IDEA N205-A**

- To learn more about the damage detection & imaging technology, please contact Dr. Didem Ozevin, Professor, University of Illinois at Chicago: dozevin@uic.edu, or visit https://cme.uic.edu/profiles/didem/
- To learn about equipment procuring options for bridge preservation / retrofit, please contact John Winfrey, CTO, PowerPolymer Solutions at jwinfrey@powerpolymer.net, or follow the link **above**.
- To learn about retrofit options for bridges (or general structures), please contact Dr. Thomas Attard, CEO, PowerPolymer Solutions at thomas.attard@powerpolymer.net, or follow the link **above**.

IMAGES

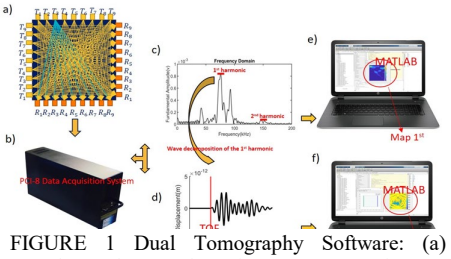

FIGURE 1 Dual Tomography Software: (a) transducer layout for given cross section: T (transmitters) and R (receivers); (b) data acquisition system; (c) frequency spectrum of receiver signal; (d) time domain signal of the fundamental wave; (e) inputs to acoustic nonlinearity coefficient-based tomography; (f) input feed to linear velocity-based

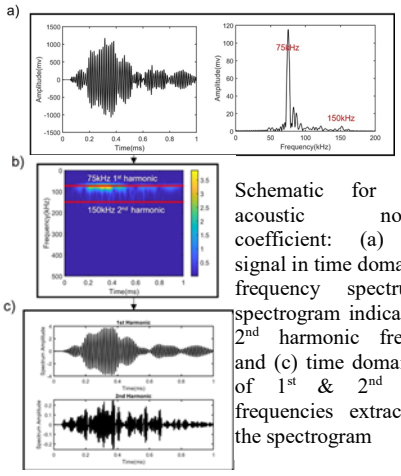

Schematic for obtaining acoustic nonlinearity coefficient: (a) received signal in time domain and its frequency spectrum; (b) spectrogram indicating 1st & 2nd harmonic frequencies; and (c) time domain signals of 1st & 2nd harmonic frequencies extracted from the spectrogram

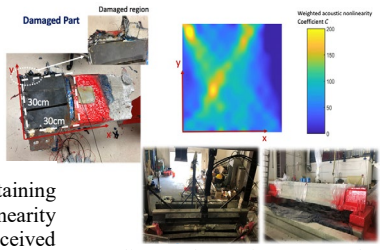

Nonlinear ultrasonic tomography measured from the damaged section of concrete girder. The support section was strengthened using the HMC polymer coating prior to loading